10-22-2002

Volcanic Mound Fields on the East Pacific Rise, 16°-19°S: Low Effusion Rate Eruptions at Overlapping Spreading Centers for the Past 1 Myr

Scott M. White

Ken C. Macdonald
University of California - Santa Barbara

John Sinton

Follow this and additional works at: https://scholarcommons.sc.edu/geol_facpub

Part of the Earth Sciences Commons

Volcanic mound fields on the East Pacific Rise, 16°–19°S: Low effusion rate eruptions at overlapping spreading centers for the past 1 Myr

Scott M. White[1] and Ken C. Macdonald
Department of Geological Sciences and Marine Science Institute, University of California, Santa Barbara, California, USA

John M. Sinton
Department of Geology and Geophysics, SOEST, University of Hawai'i at Manoa, Honolulu, Hawaii, USA

[1]   Volcanic mound fields identified on SeaMARC II and HMR1 12 kHz side-scan data from the southern East Pacific Rise (SEPR) occur near overlapping spreading centers (OSCs) and migration traces of OSCs. The volcanic mound fields appear as a distinctive hummocky seafloor fabric due to side-scan backscatter reflections from clusters of mound-shaped reflectors. The lack of growth of the mound fields away from the ridge axis, and their occurrence in association with OSC traces, suggests that mound fields form along the ridge crest near OSCs. Volcanic mound fields are found where 120 kHz side-scan and visual observations find fields of pillow mounds. Since pillow mounds are constructed by low effusion rate eruptions, the volcanic mound fields found near the OSCs and in their migration traces indicate that volcanic effusion rates tend to be lower near ridge discontinuities than midsegment regions. This tendency for low effusion rate eruptions at OSCs is documented for the past ∼1 Myr. Three independent measurements of ridge segmentation, (1) volcanic segment boundaries marked by the low effusion rate eruptions, (2) tectonic segments defined by OSCs, and (3) magmatic segment boundaries based on continuity of parental magma composition, all coincide in the study area. High backscatter off-axis lava fields not associated with seamounts are found on seafloor younger than ∼0.2 Ma. The ∼0.2 Ma corridor corroborates previous results from the distribution of small isolated volcanoes that indicates randomly distributed off-axis eruptions mainly occur on crust younger than ∼0.2 Ma.   *INDEX TERMS:* 3035 Marine Geology and Geophysics: Mid-ocean ridge processes; 3045 Marine Geology and Geophysics: Seafloor morphology and bottom photography; 3094 Marine Geology and Geophysics: Instruments and techniques; 9355 Information Related to Geographic Region: Pacific Ocean; *KEYWORDS:* spreading, ridge, segmentation, volcanic, mounds, side-scan

1. Introduction

[2] The nature of the relationship between tectonic segmentation and the volcanism at and near the ridge crest is important to understanding how ocean crust is constructed. Previous studies of crust-forming processes at fast spreading ridges include seismic observations across the ridge [e.g., *Canales et al.*, 1998; *Carbotte et al.*, 1997; *Christeson et al.*, 1994], magnetic anomaly transition widths [e.g., *Macdonald*, 1977; *Macdonald et al.*, 1983; *Sempere and Macdonald*, 1986; *Sempere et al.*, 1987], geochemical trends inferred from areally dense rock sampling [e.g., *Perfit et al.*, 1994; *Perfit and Chadwick*, 1998;

Reynolds and Langmuir, 2000; *Sinton et al.*, 1991], and theoretical approaches [*Hooft et al.*, 1996]. These studies indicate a great deal of variability in crust-forming processes, both along and across the ridge crest, at a relatively fine scale. The need for a better understanding of the variations in volcanic processes along the ridge is illustrated by the controversy over how tectonic segmentation relates to ridge magma supply. Axial segmentation of fast spreading ridges appears to be related to crustal thickness variations [*Barth and Mutter*, 1996; *Canales et al.*, 1998; *Carbotte et al.*, 2000]. However, some studies suggest that magma supply, indicated by the robustness of the axial magma chamber, is unrelated to tectonic segmentation [*Hooft et al.*, 1997; *Kent et al.*, 2000]. *White et al.* [2000] found that ridge segmentation at the third-order scale corresponds to both variations in lava effusion rate and inferred disruptions in the axial magma plumbing system. This study examines the near-ridge volcanism of

[1]Now at Department of Geological Science, University of South Carolina, Columbia, South Carolina, USA.
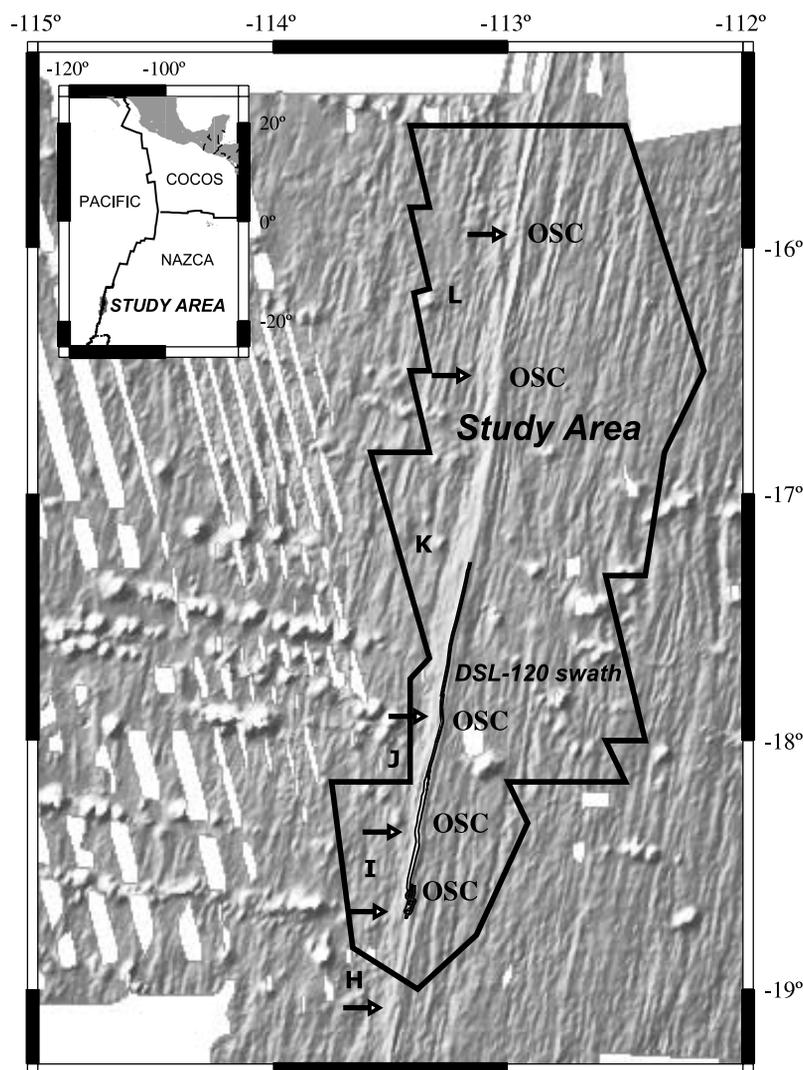
Figure 1. Shaded-relief bathymetry, false-illuminated from the northwest, showing the ridge axis, large off-axis volcanoes, and seafloor fabric in and surrounding the study area. Solid black line outlines the boundary of the study area. Along the ridge axis, the DSL-120 survey swath is outlined. Each of the overlapping spreading centers is labeled "OSC" to the right of the ridge. Arrows point to ends of magmatic segments (L-H) defined by *Sinton et al.* [1991]. Seamount chains overprint most of the seafloor just outside the study area from 17°S to 18°S. An example of anomalous abyssal hill fabric can be seen near the edge of the survey area at 17°S. Map inset shows the survey area location in the context of the local oceanic plates.

the southern East Pacific Rise (SEPR) from 15°30′S to 19°S by merging fine-scale mapping by DSL-120 sonar along the ridge crest with HMR1 and SeaMARC II 12 kHz side-scan sonar data out to ∼1 Ma crust to interpret how the relationship between volcanism and tectonic segmentation has varied over time (Figure 1).

[3] Two types of volcanic terrain in the 12 kHz side-scan sonar imagery have not been investigated previously but are common at the SEPR. One is hummocky seafloor initially identified in relict overlapping spreading center (OSC) basins by *Cormier et al.* [1996]. The other is the smooth high backscatter seafloor that has the characteristics of lava flow fields [e.g., *Macdonald et al.*, 1989]. Both of these terrain types are volcanically produced, and vastly different from the lineated, fault-bounded abyssal hills that are the

most common type of terrain on the flanks of the SEPR [*Macdonald et al.*, 1996].

1.1. Regional Geological Context

[4] Between the Garrett transform fault and the 20°40′S OSC, the axis of the SEPR forms a linear topographic high with a fairly uniform trend broken by five OSCs [*Scheirer et al.*, 1996a]. Previous studies of the SEPR have presented details of the tectonic history of the ridge [*Cormier and Macdonald*, 1994; *Cormier et al.*, 1996; *Lonsdale*, 1989] and described the distribution of the abundant off-axis volcanoes in the area [*Scheirer et al.*, 1996b; *Shen et al.*, 1995; *White et al.*, 1998]. The depth and cross-sectional area of the ridge axis in this area show one significant break at second-order OSC at 15°55′S [*Scheirer and Macdonald*,

1993]. This second-order OSC is the largest OSC in the study area, although the ridge axis is also offset by four left-stepping third-order OSCs (Figure 1). The third-order OSCs all correspond to gaps in the axial magma chamber (AMC) seismic reflector [*Detrick et al.*, 1993] and magmatic segment boundaries [*Sinton et al.*, 1991] but do not correspond to obvious long-wavelength changes in axial depth or cross-sectional area, proxies for the long-term axial magma budget [*Scheirer and Macdonald*, 1993]. *Cormier et al.* [1996] suggest that these OSCs were generated as a result of splitting of one larger OSC and are propagating along-axis at nearly 3 times the spreading rate.

[5] The great number of ridge axis discontinuities that have a well-known tectonic history makes the SEPR between 16° and 19°S an ideal place to relate off-axis seafloor morphology to similar morphology at the ridge where it has been studied at higher resolution. At the OSCs the seafloor fabric is disrupted by the interaction of the two spreading centers as the curving OSC ridge tips are decapitated and rafted onto the ridge flanks by seafloor spreading [*Macdonald et al.*, 1984]. The steep, curved ridge tips at OSCs leave a trace of discordant lineaments away from the ridge axis that have been mapped in the backscatter side-scan and bathymetric data to determine the history of tectonic segmentation [*Cormier and Macdonald*, 1994; *Cormier et al.*, 1996].

[6] Off-axis volcanism is common near the SEPR and can obscure some of the original volcanic fabric formed at the ridge axis. The extraordinarily abundant seamount chains on the west flank of the SEPR overprint the features formed at the ridge axis, but these mainly develop >10 km off-axis [*Scheirer et al.*, 1996b]. Far fewer seamount chains are found on the east flank of the ridge [*Scheirer et al.*, 1998]. Small isolated volcanoes are ubiquitous near the SEPR, but these do not obscure much area [*White et al.*, 1998].

1.2. Data Sources: HMR1, SeaMARC II, and DSL-120 Side-Scan Sonar

[7] This study focuses on the side-scan sonar backscatter imagery of volcanically produced seafloor fabric from the SEPR and its flanks, using extensive regional data collected by two near-surface towed 12 kHz side-scan systems. On R/V *Moana Wave* cruise 8710, the SeaMARC II sonar was used to map 18°–19°S in single-pass coverage on either side of the ridge axis [*Cormier and Macdonald*, 1994]. On R/V *Melville* cruise Gloria, leg 2, the HMR1 sonar was used to map 15°30′–18°S in overlapping swath coverage to obtain opposite look directions for the side-scan backscatter imagery in the map area [*Scheirer et al.*, 1996a]. Both of the 12 kHz side-scan sonar systems have similar characteristics. The SeaMARC II has a swath width of ~10 km at 3000 m seafloor depth. The HMR1 has a corresponding swath width of ~20 km. Both systems have a theoretical resolution of 50–100 m horizontal pixels depending on the angle of incidence with the seafloor of the sonar sound and depth to the seafloor. We refer to these data collectively as the 12 kHz side-scan data throughout the rest of the paper.

[8] To achieve coverage at a much higher resolution than 12 kHz side-scan, the 120 kHz side-scan DSL-120 is towed ~100 m above the bottom to obtain backscatter imagery with ~1 m horizontal pixel resolution and bathymetry with ~5 m horizontal pixel resolution and 5–10 m depth resolution over a swath width of ~1 km along the ridge crest. Features that are near the limit of resolution for the 12 kHz side-scan systems show up clearly in the DSL-120 sonar images, enhancing our sonar interpretation where coverage at two scales overlaps. Complete coverage of the ridge crest from 17°15′ to 18°40′S is available from DSL-120 surveys on R/V *Melville* cruise Sojourn, leg 2 [*White et al.*, 2000] and R/V *Atlantis* cruise 3, leg 31 [*Sinton et al.*, 2002].

[9] The limits of available sonar coverage and the lack of identifiable volcanic fabric on older seafloor define the boundaries of our study area (Figure 1). On crust older than ~1 Ma the mound fields become difficult to identify due to burial by sediment, and no lava flow fields are observed. We have excluded from the study area much of the area dominated by seamount chains from 16° to 18°S west of the ridge axis, resulting in greater overall coverage of the east flank of the ridge (Figure 1). Volcanic fabric on the flanks of seamounts is probably related to seamount-forming eruptions rather than ridge axis volcanism and is discussed in previous work [*Scheirer et al.*, 1996b; *Shen et al.*, 1995]. Therefore, we do not consider the high backscatter aprons of seamounts in this study. The study area boundaries include nearly equal coverage on both sides of the ridge axis out to ~20 km from the ridge axis enabling us to investigate the full history over >0.2 Ma and to ~1 Ma on the east flank.

2. Results

2.1. Detection of Volcanic Mounds in SeaMARC II and HMR1 Backscatter Imagery by Comparison to DSL-120 Data

[10] Along the 150 km of ridge crest where coincident 12 kHz side-scan and DSL-120 data exist, there is an excellent correlation between distinctive hummocky terrain in 12 kHz backscatter and fields of small volcanic mounds fully resolved by the DSL-120 system (Figures 2 and 3). DSL-120 sonar surveys revealed that small volcanic mounds are found in greatest abundance near OSCs and in somewhat lesser abundance near all third-order ridge discontinuities generally [*White et al.*, 2000]. Visual investigation found that these small (200 m average diameter) mounds are composed primarily of pillow lava [*Sinton et al.*, 2002; *White et al.*, 2000]. In practice, volcanic mound fields >3 km^2 were unambiguous on the 12 kHz side-scan records, while isolated mounds proved difficult to recognize in the backscatter (Figure 3).

[11] Although fields of volcanic mounds appear to be detectable, individual pillow mounds should be at or below the theoretical resolution limit of the 12 kHz side-scan data. To establish a detection threshold for individual mounds, we identified those mounds in the 12 kHz side-scan records that matched the location of a pillow mound in the DSL-120 records by comparing individual images of pillow mounds from 12 kHz side-scan with DSL-120 side-scan in a geographical information system. Some of these mounds are individuals outside the area defined by mound fields. Overall, 16% of the individual mounds in the DSL-120 records also have clearly defined reflectors in the 12 kHz side-scan records. However, the 12 kHz side-scan systems detected ~50% of pillow mounds with >60–70,000 m^2 base area or

(A.) 12 kHz HMR-1 Side-Scan
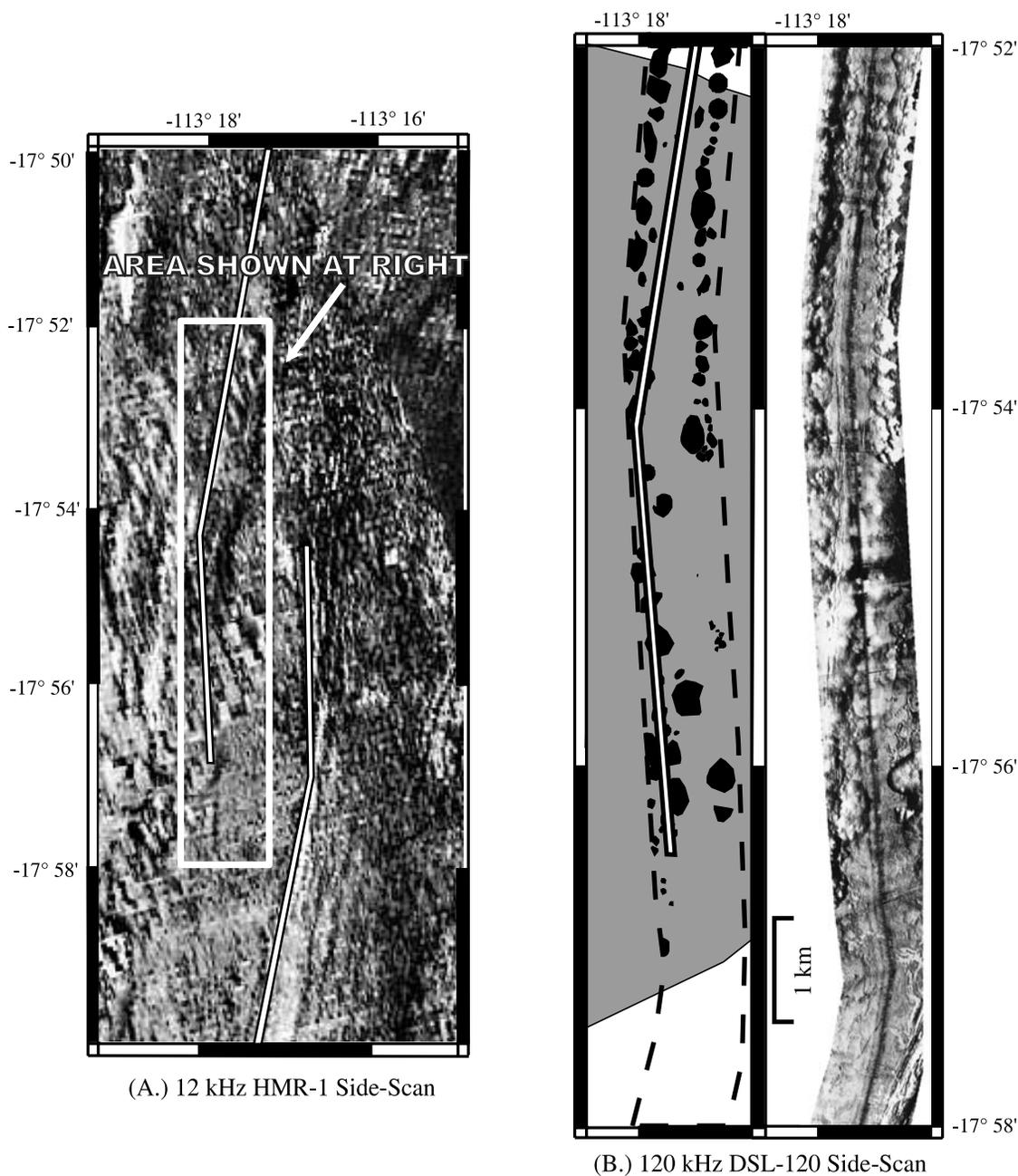
(B.) 120 kHz DSL-120 Side-Scan

Figure 2. Comparison of the mound fields resolved by 12 kHz side-scan to the pillow mounds in the DSL-120 side-scan records at the 17°55′S OSC. A double line marks the position of the ridge axis. Higher backscatter reflectivity is darker on both panels. (a) West-looking HMR-1 backscatter from the overlap region showing the hummocky seafloor along the west limb of the OSC and in the overlap basin, in contrast to the smooth backscatter return along the east limb. The white box outlines the area of DSL-120 coverage over the hummocky seafloor. (b) A magnified view of the DSL-120 data showing (right) individual mounds and (left) our interpretation of each data set. For the interpretation, pillow mounds identified on the DSL-120 record are shown as black areas, the mound fields from SeaMARC II are shaded gray areas, and the DSL-120 swath is outlined by dashed lines. The hummocky seafloor correlates very well with locations of small mounds on the DSL-120 side-scan records.

a basal diameter of ∼300 m assuming that the mounds have circular bases. At the 100 m pixel size for the 12 kHz side-scan backscatter, only 9 pixels (a 3 × 3 pixel square) would cover a 300 m diameter mound; to resolve a circular feature such as a mound requires at least a 3 × 3 square of pixels. Thus it is probable that the practical horizontal pixel

resolution of the 12 kHz backscatter data from this area is <100 m to account for the good match between >300 m diameter pillow mounds and the poorer match with the smaller mounds. For these reasons, we use the 12 kHz side-scan records to extend the record of volcanic mound fields off-axis but do not attempt to count the individual number
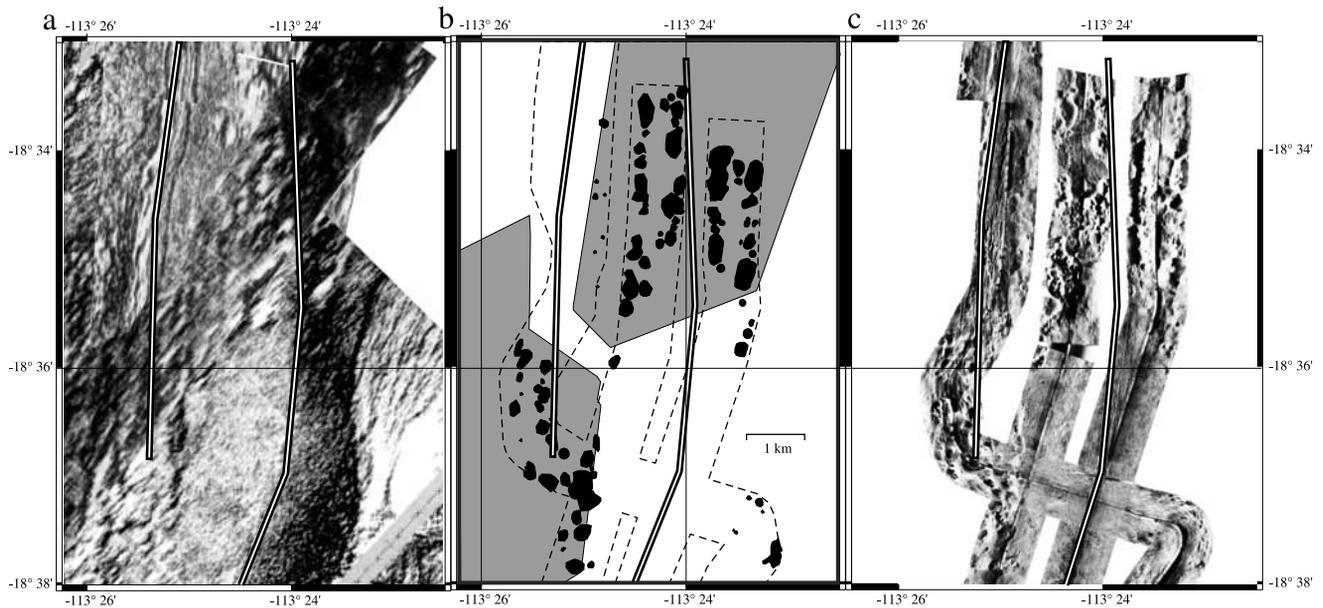
Figure 3. Comparison of the mound fields resolved by 12 kHz side-scan to the pillow mounds in the DSL-120 side-scan records at the 18°35′S OSC. Backscatter side-scan from (a) SeaMARC II, and (c) DSL-120, and (b) our sonar interpretations of each data set. The ridge axis is marked by double line. In Figure 3b, pillow mounds identified on the DSL-120 record are shown as black areas, the mound fields from SeaMARC II are shaded gray areas, and the DSL-120 swath is outlined by dashed lines. The greatest concentration of large pillow mounds in DSL-120 records occur where mound fields are identified in the 12 kHz SeaMARC II records, around the east limb and south of the west limb of the OSC. A few small pillow mounds in the easternmost DSL-120 swath are barely detectable in the SeaMARC II records but do not form part of a recognizable mound field of >3 km^2 area (see text for discussion).

of pillow mounds off-axis. Instead, we have identified the outlines of all of the volcanic mound fields clearly imaged in the 12 kHz side-scan.

2.2. Volcanic Mound Fields and Migration of OSCs

[12] Volcanic mound fields in the 12 kHz side-scan data are characterized by a hummocky seafloor fabric composed of many small mounds of fairly even size near the resolution limit of the 12 kHz side-scan data. To define the mound fields, we traced their outlines on 1:100,000 SeaMARC II and 1:200,000 HMR1 maps. We chose mound fields somewhat conservatively looking for areas of hummocky fabric large enough to be unambiguous. The smallest unambiguous volcanic mound fields were 3 km^2 in total area. Volcanic mound fields are found at each of the OSCs along the ridge axis (Figure 4).

[13] The discordant zones are areas of disturbed seafloor fabric defined by distinct continuous swaths of unusually deep grabens, very high fault scarps, and discordant lineaments (Figure 5). Discordant zones always follow the OSC migration traces identified by *Cormier et al.* [1996]. We picked the boundaries of the discordant zones based on the patterns of discordant lineaments (large scarps with trends not parallel to the abyssal hill fabric) and bathymetric anomalies (unusually deep grabens) [*Cormier et al.*, 1996], combined with an analysis of seafloor roughness. We expect higher scarps surrounding OSC fabric [*Cormier et al.*, 1996; *Crowder and Macdonald*, 2000; *Goff et al.*, 1993].

[14] The vast majority of the mound fields lie inside the discordant zones, and most of the others fall partly inside (Figure 4). Discordant zone boundaries picked entirely from tectonic criteria may miss some of the area affected volcanically by the OSC discontinuity because the volcanic mound fields often extend farther along the ridge axis than the overlap of the two ridge axes at the OSC [*White et al.*, 2000]. Discordant seafloor fabric is formed mainly where the two ridge axes overlap, but the volcanic mound fields at the ridge are found in a much larger area surrounding the OSC (Figure 4). Thus mound fields found off-axis also may be expected to extend beyond the boundaries of the tectonically defined discordant zone. If we assume that all of the mound fields that fall partially within discordant zones should be included within those discordant zones, then the total area of mound fields within the discordant zone is ~2100 km^2 (Table 1). Otherwise the area of mound fields entirely within the defined discordant zone boundaries is ~1900 km^2. The mound fields also occupy a significant area of the discordant zones but a very minor area outside of them (Table 1).

2.3. Lava Fields

[15] High-backscatter 12 kHz side-scan over large flat areas and often obscuring small fault scarps occur have been interpreted as young lava flow fields elsewhere along the EPR [e.g., *Davis et al.*, 1986; *Fornari et al.*, 1985; *Macdonald et al.*, 1989]. Fourteen of such lava fields exist within the study area, including a zone along the entire length of the ridge axis (Figure 6). The double-coverage with the HMR1
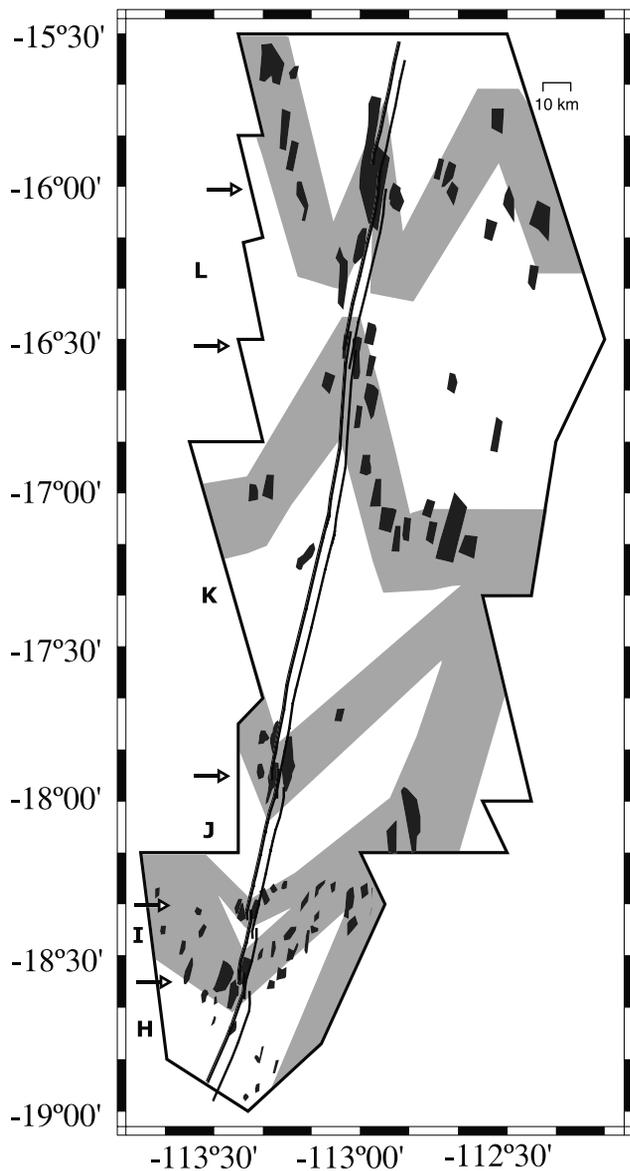
Figure 4. Map of the mound fields (dark shaded rectangles) found within the study area and discordant zones from Figure 5 in lighter shading. A heavy black line outlines the boundaries of the study area. A thin double line traces the ridge axis through the study area. The majority of mound fields lie within the discordant zones. Arrows point to ends of magmatic segments (L-H) defined by *Sinton et al.* [1991]. Magmatic segments, the OSC-bounded tectonic segments, and mound fields all coincide.

north of 18°S simplifies lava field identification because lava fields will have high backscatter return from opposite ensonification directions, while steep slopes (fault scarps) will show up from just one direction. In utilizing the SeaMARC II data south of 18°S, more care must be taken to distinguish lava flows from steep slopes. In most cases, fault scarps appear as ribbons of high backscatter return that differ from the ameboid shapes of the lava fields.

[16] The off-axis lava flow fields tabulated in this study are high backscatter 12 kHz side-scan that also lie outside of the axial high backscatter zone, and are neither part of

seamount chains nor part of the high backscatter apron around one of the isolated off-axis volcanoes (Figure 7) [*Scheirer et al.*, 1998, 1996b; *White et al.*, 1998]. This criterion excludes most of the high backscatter seafloor, because most of it occurs around seamount volcanoes [*Scheirer et al.*, 1998, 1996b]. Additionally, a continuous zone of high-backscatter surrounding the ridge axis marks a zone where repaving by lava flows is so frequent that the seafloor is essentially sediment-free to the penetration depth of the sonar (Figure 6). The average width of the axial high-backscatter corridor is ∼7 km, varying from 5 to 10 km along most of the ridge axis. We find that 7 of 14 lava fields that are contiguous with the zone of high backscatter around the ridge axis, originating on the axial topographic high and protruding onto lower backscatter (older) seafloor. These contiguous lava fields are differentiated from the high backscatter corridor generally surrounding the ridge axis
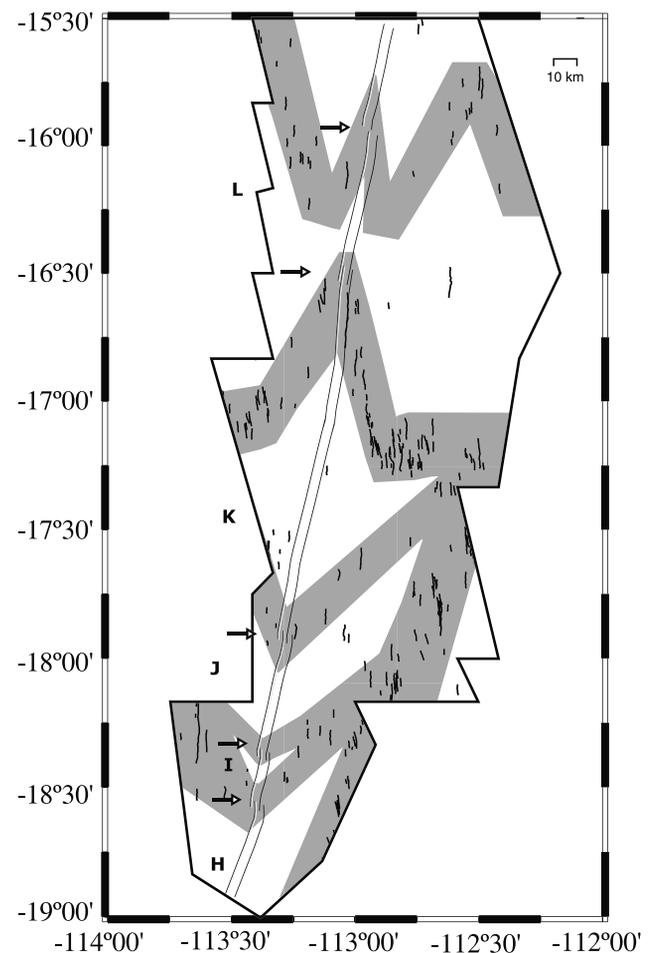

Figure 5. Map of the discordant lineaments (black lines) [*Cormier et al.*, 1996] that together with unusually high scarps and bathymetric depth anomalies [*Cormier et al.*, 1996] form the basis for identifying the discordant zones (lighter shaded regions) that are found in OSC migration traces. Definition of discordant lineaments is discussed further in the text. A heavy black line outlines the boundaries of the study area. A thin double line traces the ridge axis through the study area. Arrows point to ends of magmatic segments (L-H) defined by *Sinton et al.* [1991].

Table 1. Correlation of Mound Fields Identified From 12 kHz Side-Scan Sonar to the Discordant Zones Defined by Discordant Seafloor Fabric

	Within Discordant Zones	Outside Discordant Zones	Total
Number of mound fields	76	9	85
Area of mound fields, km^2	2095	177	2272
Percent of mound field area, %	92	8	100
Area of seafloor, km^2	16,800	21,572	38,372
Mound field area as percent of total seafloor, %	12	1	6

by having higher reflectivity than the surrounding seafloor at their edges, and by their irregular outline tending to flow between abyssal hills. We are unable to trace any of them back to the ridge axis due to insufficient reflectivity contrast. Lava fields may be evidence of rare large eruptions from the ridge axis, traversing >20 km but rarely extend more than 10 km perpendicular to the axis because the lava tends to flow along axis-parallel grabens.

[17] The lava fields are all within ~15 km of the ridge axis on crust <0.2 Ma (Figure 6). In many cases, the edges of lava fields terminate along an abyssal hill fault. Presumably, fault scarps dam and divert lava flows, indicating that this faulting preceded the lava flow emplacement.

3. Discussion

3.1. Low Effusion Rate Eruptions at Overlapping Spreading Centers and the Linkage of Tectonic, Magmatic, and Volcanic Segmentation

[18] The close association of mound fields and discordant zones from second- and third-order OSCs in the 12 kHz side-scan records corroborates previous observations that mound-forming eruptions of pillow lava are common at third-order ridge discontinuities [*White et al.*, 2000] and expands these data to include second-order discontinuities as well (note that the end of a third-order segment may be a second-order ridge discontinuity, see Figure 2 of *Macdonald et al.* [1991]). Although pillow mounds occur at all of the third-order ridge discontinuities on the SEPR, only the OSCs have sufficient size and longevity to create mound fields large enough to be identified (>3 km^2) on 12 kHz side-scan records. The finest scale third-order ridge discontinuities may be nonoverlapping offsets, existing for only a few thousand years, that rapidly reorganize and propagate before a large group of pillow mounds can form, in contrast to the largest third-order discontinuities which form OSCs where extensive groups of pillow mounds may form. It is the longevity of the OSC offsets that allows the discordant tectonic fabric and volcanic mound fields to be preserved off-axis without being overprinted by subsequent lava flows from the ridge crest. None of the smaller ridge discontinuities have sufficient size or longevity to leave a detectable off-axis trace. Furthermore, larger mound fields seem to be created at larger OSC offsets. For example, the largest mound field in our study area surrounds the large OSC at 15°55′S; very small mound fields are observed around the smallest OSCs at 16°30′S and 18°22′S. Mound fields are also ubiquitous within the discordant zones and quite rare outside of them (Table 1). The discordant zones we identified suggest that 20–25% of the seafloor in the study area is disrupted by volcanic and tectonic processes related to

OSCs. The occurrence of mound fields around OSCs is not unique to the SEPR, but has been noted in side-scan sonar studies of OSCs on the northern EPR as well [*Antrim et al.*, 1988; *Hekinian et al.*, 1985; *Macdonald et al.*, 1992; *Sempere and Macdonald*, 1986]. The SeaMARC II data from 9°–10°N show mound fields in both the overlap basin and the migration trace of the 9°03′N OSC [*Macdonald et al.*, 1992; *Sempere and Macdonald*, 1986].

[19] Throughout the study area, the mound fields show no evidence of off-axis growth (Figure 8). This is consistent with the formation of all of the mound fields near the rise axis and subsequent passive rafting off-axis. Admittedly, we cannot detect if a few new individual mounds do form. However, if off-axis volcanic activity in the mound fields were common, it would likely produce either large volcanic edifices consistently in discordant zones or systematically larger mound fields farther from the ridge axis. Instead, the average size of the mound fields remains fairly constant, within one standard deviation of the mean mound field area, and slightly fewer mound fields are found with increasing distance off axis (Figure 8). Additionally, the mound fields become difficult to identify from side-scan imagery on crust older than ~1 Ma (used as one of the constraints on our study area boundaries), and most seem to fade from the 12 kHz side-scan records somewhere near the 1 Ma isochron. Estimated sediment accumulation rates range widely, but near-axis rates of 2–10 cm/kyr [*Dekov and Kuptsov*, 1994; *Lyle et al.*, 1987; *Marchig et al.*, 1986] suggest that in ~1 Myr, sediment thickness would obscure or completely bury small (<20 m high) volcanic mounds so long as no new mounds were forming. The volcanic mound fields have very similar backscatter appearance and a wide size distribution of mounds that are randomly distributed within each of the mound fields if our observations based on DSL-120 sonar may be applied off-axis. Mound fields may become obscured relatively simultaneously as sediment fills in, around, and finally over most of the mounds, rather than disappearing gradually by shrinking through time or small mound fields disappearing long before large ones. Thus mound fields found off-axis most likely are relict features of past disruptions to the axial volcanic system. These disruptions to the axial volcanic system have occurred at OSCs within the study area for at least the last 1 Myr (Figure 5).

[20] The systematic formation of volcanic mound fields at OSCs implies that eruptions tend to have lower effusion rates near OSCs than elsewhere along the ridge. Mound fields are groups of pillow mounds as explained earlier [*Sinton et al.*, 2002; *White et al.*, 2000]. Pillow lava and, thus, pillow mounds are inferred to form at the lowest lava effusion rates [*Bonatti and Harrison*, 1988; *Gregg and Fink*, 1995; *Griffiths and Fink*, 1992]. Outside of the areas
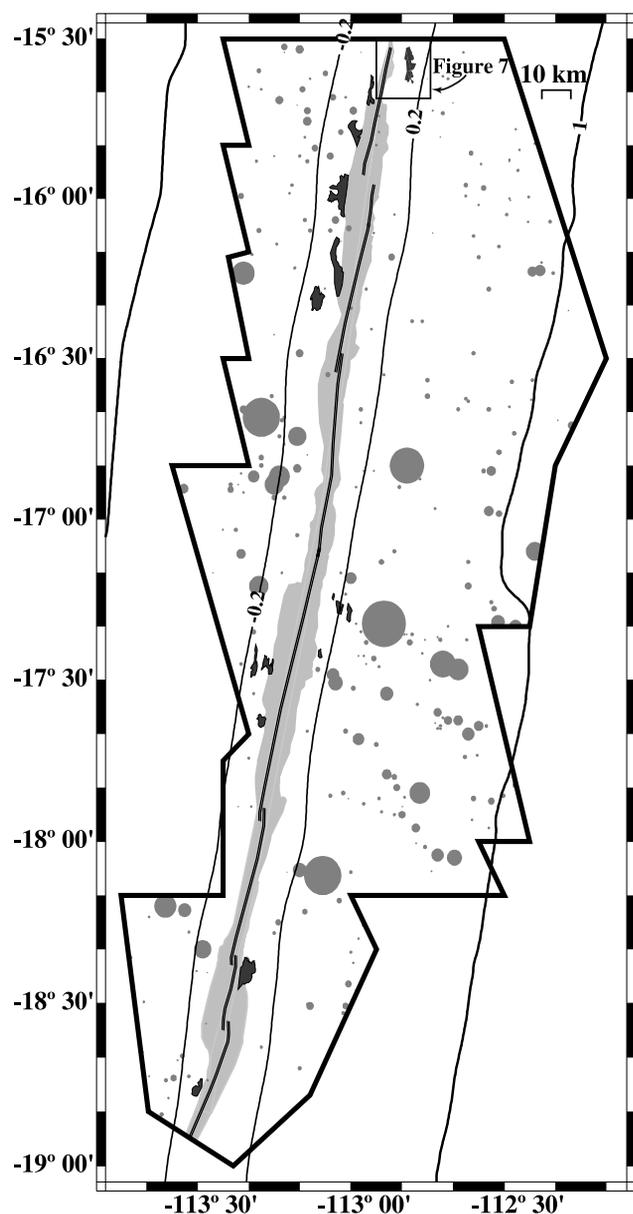
Figure 6. Map of all of the lava fields in the study area that are not associated with off-axis volcanoes. Lava fields are shown as black areas. Off-axis volcanoes are idealized as gray shaded circles scaled to the basal diameter of the volcano [*White et al.*, 1998]. The thick black line marks the boundary of the study area. Slightly thinner black lines are 0.2 Ma and 1 Ma isochrons interpolated as by *Cormier et al.* [1996] from magnetic isochron picks (D. Wilson, personal communication, 2000). Lava fields are only found close to the ridge axis, on crust less than ∼0.2 Ma. The light gray shading shows the high-backscatter zone surrounding the ridge axis (shown as thin black double line) picked from 12 kHz sonar data.

of pillow mounds near the second- and third-order ridge discontinuities, higher effusion rate lobate lava flows are generally the most common lava morphology on the SEPR [*Auzende et al.*, 1996; *Renard et al.*, 1985; *Sinton et al.*, 2002; *White et al.*, 2000].

[21] One possible factor contributing to the inferred reduction in lava effusion rates is the decrease in spreading rate on the ridge axes within OSCs. The spreading rate at the ridge axis on each limb of the OSC decreases because the sum of the spreading rate for both spreading centers in the overlap zone must not be greater than the full spreading rate. Because the seafloor just beyond the OSC rift tip is not spreading at all but the ridge axis behind the OSC is rifting at the total spreading rate, the spreading rate along the OSC limb must decrease approaching the OSC tip [*Macdonald et al.*, 1984]. In effect, each limb of the OSC acts as a slower spreading rate ridge axis [*Macdonald et al.*, 1988]. This is a satisfying explanation since slow spreading ridges seem to erupt more pillow lava than fast spreading ridges [e.g., *Perfit and Chadwick*, 1998] but only explains mound fields occurring within the overlap zone. However, the link between spreading rate and lava morphology cannot explain why mound fields extend along the ridge axis beyond the overlap zone between the two ridge axes.

[22] Disruptions to the shallow magma delivery system, manifested by breaks in the AMC, may result in the development of mound fields at OSCs. The absence of a steady state AMC is common at OSCs on the EPR [*Detrick et al.*, 1987, 1993]. Petrologic data also suggest that separate, disconnected magma chambers exist on either side of the OSCs in our study area [*Sinton et al.*, 1991]. Recent geologic mapping suggests pillow mounds tend to be found along-strike at the end of eruptive units defined by *Sinton et al.* [2002]. On the EPR the disappearance of the AMC at ridge discontinuities is often accompanied by an increase in crustal thickness [*Barth and Mutter*, 1996; *Canales et al.*, 1998; *Cormier et al.*, 1995; *Scheirer et al.*, 1998]. These changes in crustal structure affect a region much larger than the overlap between the two ridge axes at OSCs. Disruptions to the AMC appear correlated with existence of pillow mounds along the SEPR [*White et al.*, 2000]. The lack of a steady state AMC may indicate a lower magma pressure and thicker brittle lid, leading to a reduction in the width of eruptive dikes. Small changes in dike width can produce large changes in the lava effusion rate at eruption, controlling the overall morphology of volcanic vent structures [*Head et al.*, 1996]. Also, a reduction in magma pressure or an increase in viscosity will lead to lower lava effusion rates at a constant dike width. The predominance of pillow lava and pillow mounds on the EPR in areas where an AMC is not detected suggests that magma delivery is generally impeded at OSCs relative to the midsegment regions.

[23] Tectonic, magmatic, and volcanic segment boundaries all coincide in the study area to within the limits of the resolution of each data set. These data sets indicate the locations of ridge discontinuities from three independent measurements. *Cormier et al.* [1996] and *Scheirer et al.* [1996a] use multibeam and side-scan sonar data to describe the OSC-bounded tectonic segments of the ridge based on the morphological and structural criteria of *Macdonald et al.* [1988]. *Sinton et al.* [1991] define magmatic segments based on the along-axis continuity of volcanic glass samples with similar parental magmas. Samples from dredges made 10–15 km apart along-axis were used to define magmatic segmentation, limiting the resolution to segments >20 km long. This sample spacing defines magmatic segments that coincide with the OSC-bounded segments. Volcanic seg-
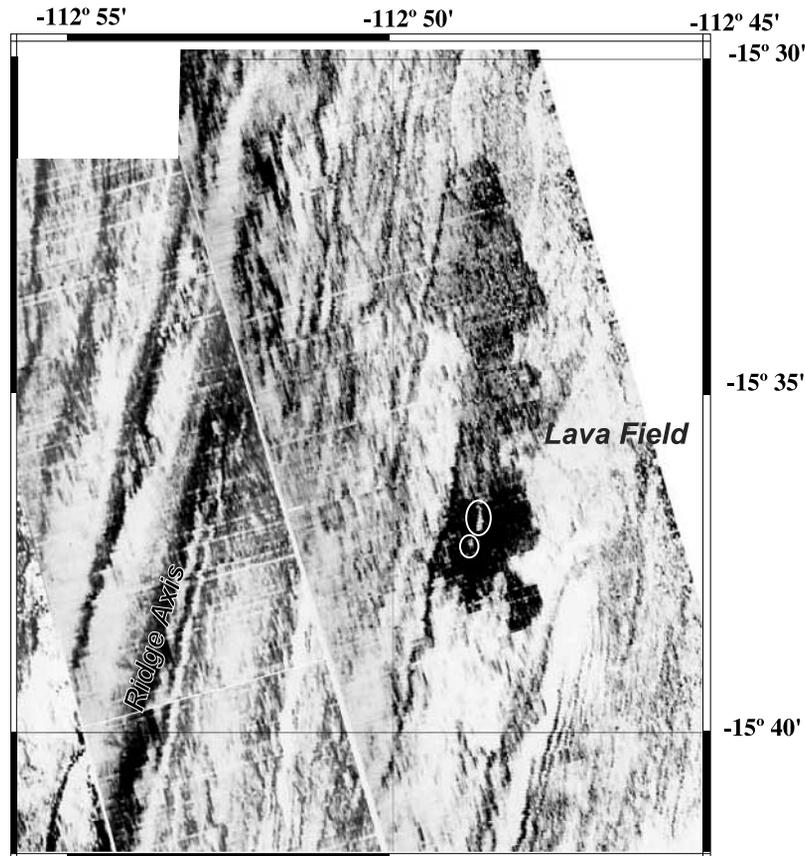
Figure 7. A typical lava field in HMR1 side-scan sonar appears on the right side as an irregularly shaped darker area dammed against an abyssal hill scarp to the west. Higher-backscatter reflectivity is darker shaded. This sonar mosaic was made from three west looking swaths running northwest. The two different shades of backscatter reflectivity in the lava field may indicate that at least two lava flows comprise this field. The white circles highlight two tiny mounds that might be the source for this field. Very small mounds were found on many of the lava fields in this study but are not resolved by multibeam bathymetry.

mentation is inferred from the distribution of volcanic mound fields following the volcanic segmentation based on inferred volcanic effusion rate [*White et al.*, 2000]. The 12 kHz side-scan resolves mound fields >3 km^2 in area. This level of resolution defines volcanic segmentation that occurs at the OSCs and exists in their migration traces.

3.2. Across-Axis Width of Volcanic Emplacement

[24] Frequent volcanic activity seems to continue out to a crustal age of 0.2 Ma on the SEPR. This crustal age limit, corresponding to a distance of ~15 km off axis, is the zone where lava fields are found, isolated off-axis volcanoes form, and most seamount chains initiate [*Scheirer et al.*, 1996b; *White et al.*, 1998]. The <0.2 Ma crust zone of frequent, isolated eruptions was found to apply independent of spreading rate for the northern EPR [*Alexander and Macdonald*, 1996] and Mid-Atlantic Ridge [*Smith and Cann*, 1999], suggesting that lithospheric penetrability may control off-axis eruptions [*White et al.*, 1998].

[25] On crust younger than 0.2 Ma, lava fields, isolated volcanoes, and seamount chains together resurface up to 8–10% of the seafloor outside of the area of the neovolcanic zone. Lava fields alone resurface a total area of 250–260 km^2 (~3% of the seafloor), although they create no edifices
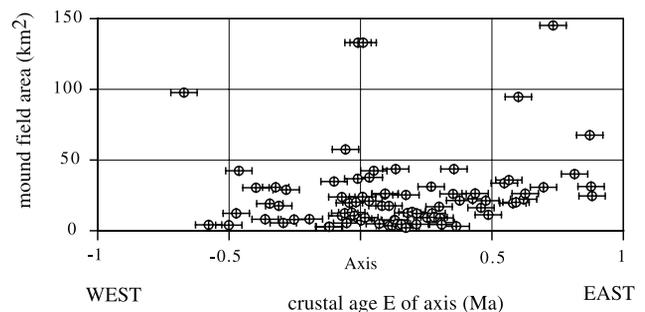

Figure 8. Sizes of the mound fields, in square kilometers of area, compared to the age of the crust near the centroid of the mound field. Crustal age is interpolated as by *Cormier et al.* [1996] from magnetic isochron picks (D. Wilson, personal communication, 2000). Error bars represent 0.1 Ma age uncertainty due to the size of the mound fields and the accuracy of the age interpolation. The error bars on the area represent standard error (~3 km^2). One standard deviation from the mean size encompasses mound fields of 4–80 km^2 area. No statistically significant variation of mound field size with seafloor age is observed within the study area, suggesting that the mound fields are created at or near the EPR axis.

within the resolution limits of multibeam bathymetry. The lava fields individually cover areas ranging from 1 to 45 km^2 with an average area of 16 km^2 which is an order of magnitude smaller than the 220 km^2 lava field mapped at 8°S on the EPR [*Macdonald et al.*, 1989]. Although off-axis eruptions can be quite extensive, large eruptions seem to be unusual and do not systematically thicken the crust (except locally at seamounts). Thus the vast majority of the oceanic crust is formed within the neovolcanic zone.

[26] The presence of long lava fields that may originate at the ridge axis suggests that the SEPR has two distinct eruptive styles: (1) frequent short, low volume eruptions and (2) rare long, higher volume lava flows. Modeling crustal emplacement to fit the shape of the base of seismic layer 2A on the SEPR, *Hooft et al.* [1996] found the best match was a bimodal distribution lava flow lengths with 95% of lava flows ~50 m long and 5% of lava flows emplaced 0.5 km off-axis and ~1 km long. The idea that eruptive behavior of the EPR may be bimodal is also implied in multistage models for the formation of axial summit troughs [*Fornari et al.*, 1998; *Lagabrielle and Cormier*, 1999]. The lava flow fields, especially those contiguous with the high-backscatter zone at the ridge, are possible evidence for rare voluminous eruptions from the SEPR. Ridge morphology is weakly correlated to the width of the high-backscatter zone surrounding the ridge axis. For instance, both width of the high-backscatter zone and axial cross-sectional area are small north of the 15°55'S OSC and large around 17°30'S (Figure 7). However, ridge morphology is relatively uniform within the study area [*Scheirer and Macdonald*, 1993]. Unfortunately, we cannot distinguish between long and short flows because most lava flows look equally young on the high-backscatter 12 kHz sonar images near the ridge axis. Further work defining and mapping products of individual eruptions is needed to accurately determine a size:frequency ratio for mid-ocean ridge eruptions.

4. Conclusions

[27] On the basis of HMR1 and SeaMARC II side-scan sonar data from the SEPR, our results suggest that volcanic mound fields coincide with major disruptions to the axial volcanic system inferred from the structural and magmatic segmentation of the ridge [*Cormier et al.*, 1996; *Sinton et al.*, 1991]. Our primary results concern association of volcanic features with segmentation and crustal accretion along the SEPR:

1. The hummocky seafloor fabric in HMR1 and SeaMARC II side-scan sonar is caused by fields of small pillow mounds. These mound fields form near the axis, and have been imaged there with DSL-120 sonar. Volcanic mound fields within the neovolcanic zone are located near OSCs.

2. The areas of the mound fields do not increase with age or distance from the ridge axis implying that mound fields are formed near the ridge and do not commonly continue to be volcanically active away from the ridge axis. Volcanic mound fields are a manifestation of disruptions to the axial structure corresponding to the magmatic segmentation defined by *Sinton et al.* [1991]. The lack of mound fields outside OSC discordant zones suggests that the present association between the segmentation of the volcanic systems and ridge axis morphology has been maintained through time. Off-axis volcanoes and seamounts initiate independently of the pillow mounds.

3. Volcanic mound fields are inferred to form as a result of decreased volcanic effusion rates around volcanic segment ends (second or third order ridge discontinuities) on the SEPR. The close association of mound fields with discordant zones illustrates that the effusion rate systematically decreases at discontinuities that are large enough to leave an off-axis discordant zone.

4. Isolated, off-axis lava fields are patches of high backscatter seafloor in the SeaMARC II and HMR1 sonar data. Lava fields occur only on crust <0.2 Ma, within the same zone where isolated off-axis volcanoes form and grow [*White et al.*, 1998] and most seamount chains initiate [*Scheirer et al.*, 1996b]. Random off-axis eruptions appear to be commonplace on the flanks of the SEPR on <0.2 Ma crust. However, these off-axis eruptions probably add very little volume to the oceanic crust.

References

Alexander, R. T., and K. C. Macdonald, Small off-axis volcanoes on the East Pacific Rise, *Earth Planet. Sci. Lett.*, *139*, 387–394, 1996.

Antrim, L., J.-C. Sempere, K. C. Macdonald, and F. N. Spiess, Fine scale study of a small overlapping spreading center system at 12°54'N on the East Pacific Rise, *Mar. Geophys. Res.*, *9*, 115–130, 1988.

Auzende, J. M., V. Ballu, R. Batiza, D. Bideau, J. L. Charlou, M.-H. Cormier, Y. Fouquet, P. Geistdoerfor, Y. Lagabrielle, J. Sinton, and P. Spadea, Recent tectonic, magmatic and hydrothermal activity on the East Pacific Rise between 17° and 19°S: Submersible observations, *J. Geophys. Res.*, *101*, 17,995–18,010, 1996.

Barth, G. A., and J. C. Mutter, Variability in oceanic crustal thickness and structure: Multichannel seismic reflection results from the northern East Pacific Rise, *J. Geophys. Res.*, *101*, 17,951–17,975, 1996.

Bonatti, E., and C. G. A. Harrison, Eruption style of basalt in oceanic spreading ridges and seamounts: Effect of magma temperature and viscosity, *J. Geophys. Res.*, *93*, 2967–2980, 1988.

Canales, J. P., R. S. Detrick, S. Bazin, A. J. Harding, and J. A. Orcutt, Off-axis crustal thickness across and along the East Pacific Rise within the MELT area, *Science*, *280*, 1218–1220, 1998.

Carbotte, S. M., J. C. Mutter, and L. Xu, Contribution of volcanism and tectonism to axial and flank morphology of the southern East Pacific Rise, 17°10'–17°40'S, from a study of layer 2A geometry, *J. Geophys. Res.*, *102*, 10,165–10,184, 1997.

Carbotte, S. M., A. Solomon, and G. Ponce-Correa, Evaluation of morphological indicators of magma supply and segmentation from a seismic reflection study of the East Pacific Rise, 15°30'–17°N, *J. Geophys. Res.*, *105*, 2737–2760, 2000.

Christeson, G. L., G. M. Purdy, and G. J. Fryer, Seismic constraints on shallow crustal emplacement processes at the fast spreading East Pacific Rise, *J. Geophys. Res.*, *99*, 17,957–17,973, 1994.

Cormier, M.-H., and K. C. Macdonald, East Pacific Rise 18°S–19°S: Asymmetric spreading and ridge reorientation by ultra-fast migration of ridge axis discontinuities, *J. Geophys. Res.*, *99*, 543–564, 1994.

Cormier, M. H., K. C. Macdonald, and D. S. Wilson, A three-dimensional gravity analysis of the East Pacific Rise from 18°–21°30'S, *J. Geophys. Res.*, *100*, 8063–8082, 1995.

Cormier, M.-H., D. S. Scheirer, and K. C. Macdonald, Evolution of the East Pacific Rise at 16°–19°S since 5 Ma: Bisection of OSC's by new rapidly propagating ridge segments, *Mar. Geophys. Res.*, *18*, 52–84, 1996.

Crowder, L. K., and K. C. Macdonald, New constraints on the width of the zone of active faulting on the East Pacific Rise 8°30′N–10°N from Sea Beam bathymetry and SeaMARC II side-scan sonar, *Mar. Geophys. Res.*, *21*, 513–527, 2000.

Davis, E. E., R. G. Currie, B. S. Sawyer, and J. G. Kosalos, The use of swath bathymetric and acoustic image mapping tools in marine geoscience, *Mar. Technol. Soc. J.*, *20*, 17–27, 1986.

Dekov, V. M., and V. M. Kuptsov, Late Quarternary rates of accumulation of metal-bearing sediments on the East Pacific Rise, *Oceanology*, *32*, 94–101, 1994.

Detrick, R. S., P. Buhl, E. Vera, J. Mutter, J. Orcutt, J. Madsen, and T. Brocher, Multi-channel seismic imaging of a crustal magma chamber along the East Pacific Rise, *Nature*, *326*, 35–41, 1987.

Detrick, R. S., A. J. Harding, G. M. Kent, J. A. Orcutt, J. C. Mutter, and P. Buhl, Seismic structure of the southern East Pacific Rise, *Science*, *259*, 499–503, 1993.

Fornari, D. J., W. B. F. Ryan, and P. J. Fox, Sea-floor lava fields on the East Pacific Rise, *Geology*, *13*, 413–416, 1985.

Fornari, D. J., R. M. Haymon, M. R. Perfit, T. K. P. Gregg, and M. H. Edwards, Axial summit trough of the East Pacific Rise 9°N to 10°N: Geological characteristics and evolution of the axial zone on fast-spreading mid-ocean ridges, *J. Geophys. Res.*, *103*, 9827–9855, 1998.

Goff, J. A., A. Malinverno, D. J. Fornari, and J. R. Cochran, Abyssal hill segmentation: Quantitative analysis of the East Pacific Rise Flanks 7°S–9°S, *J. Geophys. Res.*, *98*, 13,851–13,862, 1993.

Gregg, T. K. P., and J. H. Fink, Quantification of submarine lava-flow morphology through analog experiments, *Geology*, *23*, 73–76, 1995.

Griffiths, R. W., and J. A. Fink, Solidification and morphology of submarine lavas; a dependence on extrusion rate, *J. Geophys. Res.*, *97*, 19,729–19,737, 1992.

Head, J. W., L. Wilson, and D. K. Smith, Mid-ocean ridge eruptive vent morphology and substructure: Evidence for dike widths, eruption rates, and the evolution of eruptions and axial volcanic ridges, *J. Geophys. Res.*, *101*, 28,265–28,280, 1996.

Hekinian, R., J. M. Auzende, J. Francheteau, P. Gente, W. B. F. Ryan, and E. S. Kappel, Offset spreading centers near 12 53′N on the East Pacific Rise: Submersible observations and composition of the volcanics, *Mar. Geophys. Res.*, *7*, 329–358, 1985.

Hooft, E. E. E., H. Schouten, and R. S. Detrick, Constraining crustal emplacement processes from the variation in seismic layer 2A thickness at the East Pacific Rise, *Earth Planet. Sci. Lett.*, *142*, 289–309, 1996.

Hooft, E. E., R. S. Detrick, and G. M. Kent, Seismic structure and indicators of magma budget along the Southern East Pacific Rise, *J. Geophys. Res.*, *102*, 27,319–27,340, 1997.

Kent, G. M., et al., Evidence from three-dimensional seismic reflectivity images for enhanced melt supply beneath mid-ocean ridge discontinuities, *Nature*, *406*, 614–618, 2000.

Lagabrielle, Y., and M.-H. Cormier, Formation of large summit troughs along the East Pacific Rise as collapse calderas: An evolutionary model, *J. Geophys. Res.*, *104*, 12,971–12,988, 1999.

Lonsdale, P., Segmentation of the Pacific-Nazca spreading center, 1°N–20°S, *J. Geophys. Res.*, *94*, 12,197–12,226, 1989.

Lyle, M., M. Leinen, R. M. Owen, and D. K. Rea, Late Tertiary history of hydrothermal deposition at the East Pacific Rise, 19°S: Correlation to volcano-tectonic events, *Geophys. Res. Lett.*, *14*, 595–598, 1987.

Macdonald, K. C., Near-bottom magnetic anomalies, asymmetric spreading, oblique spreading, and tectonics of the Mid-Atlantic Ridge near lat 37N, *Geol. Soc. Am. Bull.*, *88*, 541–555, 1977.

Macdonald, K. C., S. P. Miller, B. P. Luyendyk, T. M. Atwater, and L. Shure, Investigation of a Vine-Matthews magnetic lineation from a submersible: The source and character of marine magnetic anomalies, *J. Geophys. Res.*, *88*, 3403–3418, 1983.

Macdonald, K. C., J.-C. Sempere, and P. J. Fox, East Pacific Rise from Siqueiros to Orozco Fracture Zones: Along-strike continuity of axial neovolcanic zone and structure and evolution of overlapping spreading centers, *J. Geophys. Res.*, *89*, 6049–6069, 1984.

Macdonald, K. C., P. J. Fox, L. J. Perram, M. F. Eisen, R. M. Haymon, S. P. Miller, S. M. Carbotte, M.-H. Cormier, and A. N. Shor, A new view of the mid-ocean ridge from the behaviour of ridge-axis discontinuities, *Nature*, *335*, 217–225, 1988.

Macdonald, K. C., R. Haymon, and A. Shor, A 220 km2 recently erupted lava field on the East Pacific Rise near lat 8°S, *Geology*, *17*, 212–216, 1989.

Macdonald, K. C., D. S. Schierer, and M.-H. Cormier, Mid-ocean ridges: Discontinuities, segments, and giant cracks, *Science*, *253*, 985–994, 1991.

Macdonald, K. C., P. J. Fox, S. Carbotte, M. Eisen, S. Miller, L. Perram, D. Scheirer, S. Tighe, and C. Weiland, The East Pacific Rise and its flanks, 8°–18°N: History of segmentation, propagation and spreading direction based on SeaMARC II and Sea Beam studies, *Mar. Geophys. Res.*, *14*, 299–344, 1992.

Macdonald, K. C., P. J. Fox, R. T. Alexander, R. Pockalny, and P. Gente, Volcanic growth faults and the origin of Pacific abyssal hills, *Nature*, *380*, 125–129, 1996.

Marchig, V., J. Erzinger, and P. M. Heinze, Sediment in the black smoker area of the East Pacific Rise, *Earth Planet. Sci. Lett.*, *79*, 93–106, 1986.

Perfit, M. R., and W. W. Chadwick, Magmatism at mid-ocean ridges: constraints from volcanological and geochemical investigations, in *Faulting and Magmatism at Mid-ocean Ridges*, *Geophys. Monogr. Ser.*, vol. 106, edited by W. R. Buck et al., pp. 59–116, AGU, Washington, D. C., 1998.

Perfit, M. R., D. J. Fornari, M. C. Smith, J. F. Bender, C. H. Langmuir, and R. M. Haymon, Small-scale spatial and temporal variations in mid-ocean ridge crest magmatic processes, *Geology*, *22*, 375–379, 1994.

Renard, V., R. Hekinian, J. Francheteau, R. D. Ballard, and H. Backer, Submersible observations at the axis of the ultra fast spreading East Pacific Rise (17°30′ to 21°30′S), *Earth Planet. Sci. Lett.*, *88*, 339–353, 1985.

Reynolds, J. R., and C. H. Langmuir, Identification and implications of off-axis lava flows around the East Pacific Rise, *Geochem. Geophys. Geosys.*, *1*(Article), 1999GC000033 [13,181 words], 2000.

Scheirer, D. S., and K. C. Macdonald, Variation in cross-sectional area of the axial ridge along the East Pacific Rise: Evidence for the magamatic budget of a fast-spreading center, *J. Geophys. Res.*, *98*, 7871–7885, 1993.

Scheirer, D. S., K. C. Macdonald, D. W. Forsyth, S. P. Miller, D. W. Wright, and M.-H. Cormier, A map series of the southern East Pacific Rise and it's flanks, 15°S to 19°S, *Mar. Geophys. Res.*, *18*, 1–12, 1996a.

Scheirer, D. S., K. C. Macdonald, D. W. Forsyth, and Y. Shen, Abundant seamounts of the Rano Rahi seamount field near the southern East Pacific Rise, 15° to 19°S, *Mar. Geophys. Res.*, *18*, 13–52, 1996b.

Scheirer, D. S., D. W. Forsyth, M.-H. Cormier, and K. C. Macdonald, Shipboard geophysical indications of asymmetry and melt production beneath the East Pacific Rise near the MELT Experiment, *Science*, *280*, 1221–1224, 1998.

Sempere, J.-C., and K. C. Macdonald, Deep-Tow studies of the overlapping spreading centers at 9°03′N on the East Pacific Rise, *Tectonics*, *5*, 881–900, 1986.

Sempere, J.-C., K. C. Macdonald, S. P. Miller, and L. Shure, Detailed study of the Brunhes/Matuyama reversal boundary on the East Pacific Rise at 19°30′S: Implications for crustal emplacement processes at an ultra fast spreading center, *Mar. Geophys. Res.*, *9*, 1–23, 1987.

Shen, Y., D. S. Scheirer, D. W. Forsyth, and K. C. Macdonald, Trade-off in production between adjacent seamount chains near the East Pacific Rise, *Nature*, *373*, 140–143, 1995.

Sinton, J. M., S. M. Smaglik, J. J. Mahoney, and K. C. Macdonald, Magmatic processes at superfast spreading mid-ocean ridges: Glass compositional variations along the East Pacific Rise 13°–23°S, *J. Geophys. Res.*, *96*, 6133–6155, 1991.

Sinton, J. M., E. Bergmanis, K. Rubin, R. Batiza, T. K. P. Gregg, K. Gronvold, K. Macdonald, and S. White, Volcanic eruptions on mid-ocean ridges: New evidence from the superfast spreading East Pacific Rise, 17°–19°S, *J. Geophys. Res.*, *107*(B6), 2115, doi:10.1029/2000JB000090, 2002.

Smith, D. K., and J. R. Cann, Constructing the upper crust of the Mid-Atlantic Ridge: A reinterpretation based on the Puna Ridge, Kilauea Volcano, *J. Geophys. Res.*, *104*, 25,379–25,400, 1999.

White, S. M., K. C. Macdonald, D. S. Scheirer, and M.-H. Cormier, Distribution of isolated volcanoes on the flanks of the East Pacific Rise, 15.3°–20°S, *J. Geophys. Res.*, *103*, 30,371–30,384, 1998.

White, S. M., K. C. Macdonald, and R. M. Haymon, Basaltic lava domes, lava lakes, and volcanic segmentation of the southern East Pacific Rise, *J. Geophys. Res.*, *105*, 23,519–23,536, 2000.

————————————

K. C. Macdonald, Department of Geological Sciences and Marine Science Institute, University of California, Santa Barbara, CA 93106, USA. (macdonald@geol.ucsb.edu)

J. M. Sinton, Department of Geology and Geophysics, SOEST, University of Hawai'i at Manoa, 1680 East-West Road, Honolulu, HI 96822, USA. (sinton@soest.hawaii.edu)

S. M. White, Department of Geological Sciences, University of South Carolina, 701 Sumter Street, Columbia, SC 29208, USA. (swhite@sc.edu)